JMEPEG (2010) 19:314–324
DOI: 10.1007/s11665-009-9497-4

1059-9495/$19.00

A General Algorithm for Inverse Modeling of Layer-By-Layer Liquid-Metal Deposition

S.G. Lambrakos and K.P. Cooper

(Submitted March 20, 2009)

In order that freeform fabrication techniques, which entail layer-by-layer liquid-metal deposition, transition from prototyping to manufacturing, these techniques must be made reliable and consistent. Accordingly, detailed microstructural and thermal characterizations of the structures produced are needed in order to advance these fabrication techniques. The inherent complexity of layer-by-layer liquid-metal deposition, which is characteristic of energy and mass deposition processes in general, is such that process modeling based on basic theory alone, which represents the direct-problem approach, is extremely difficult. A general approach to overcoming the difficulties associated with this inherent complexity is the inverse problem approach. Presented here is a general algorithmic structure for inverse modeling of heat transfer that occurs during layer-by-layer fabrication. This general algorithmic structure represents an extension and refinement of an algorithmic structure presented previously and is potentially adaptable for prediction of temperature histories within parts having complex geometries and for the construction of process-control algorithms.

Keywords modeling processes, powder metallurgy, shaping

1. Introduction

The many benefits of fabrication techniques based on layer-by-layer deposition processes, or solid freeform fabrication, follow from the ability to make spare or replacement parts on demand, to repair damaged parts and to add features on existing parts. Different types of layer-by-layer deposition processes, which entail droplet-by-droplet liquid-metal deposition, have been developed. Droplet-by-droplet liquid-metal deposition involves building three dimensional, net-shape metallic structures. Accordingly, a CAD solid model of the object or part is sliced into layers. Each slice or layer is formed by overlapping several reinforced melt bead droplets, which are made by continuously feeding powder or wire into a melt pool formed by a laser or electron beam. Each droplet follows the trajectory set by an automated process planner. The general droplet-by-droplet deposition process is described schematically in Fig. 1. Concentrically arranged nozzles feed metal powder or wire into a liquid-metal melt pool generated by means of either an electron or laser beam. As the substrate is translated according to a specified sequence of finite translations in the x and y directions, overlapping melt bead droplets form the first layer. The substrate is then incrementally lowered in the z direction and a second layer is formed again by a specified sequence of finite translations of the substrate in the x and y directions. This sequence of steps is continued until a three-dimensional solid object is created, which is an exact replica of the original CAD model. By this means, it is possible to fabricate fully dense, complex shape structural and functional parts with internal geometries and overhangs. References 1-9 and references therein provide a comprehensive initial survey of various aspects of layer-by-layer liquid-metal deposition processes. A brief review of some of these aspects is as follows.

Processes that entail droplet-by-droplet liquid-metal deposition are capable of fabricating metallic parts from a variety of alloys. Stainless steel, tool steel, titanium, rhenium, aluminum, and nickel-based superalloys are some of the alloys that have been successfully processed. There are potential applications for these processes in the automotive, energy, aerospace, defense, and biomedical industries where prototype parts are routinely made. The manufacture of load-bearing and functional parts, however, is faced with technical and economic hurdles. As layer-by-layer fabrication techniques mature, however, i.e., these techniques become affordable and their technical problems solved, more applications should be forthcoming. For reliability in manufacturing and consistency in part performance, droplet-by-droplet deposition of liquid metal with precise closed loop process control must be developed. For process control, it is important to understand the evolution of the microstructure, which is correlated with the nature and magnitude of the thermal fields. For example, a freeform-fabricated rectangular coupon is made by a straight-line build-up process, i.e., depositing metal on a substrate which is translated back and forth. As described in this study, the freeform-fabricated coupon is made up of several layers defined by the ripples on the surface (see Fig. 2). The surface ripples are remnants of surface tension-driven spherical melt pools, which are correlated with liquid-metal droplets. The size and shape of the surface ripples depend upon the surface tension, density of the alloy, the size of the melt pool generated by each droplet, and the fluid dynamics of the melt pools. All of which depend upon the heat input and temperature distribution.

S.G. Lambrakos and **K.P. Cooper**, Naval Research Laboratory, Materials Science and Technology Division, Washington, DC. Contact e-mail: lambrakos@anvil.nrl.navy.mil.

Among the process parameters for fabrication of net-shape metallic parts by droplet-by-droplet liquid-metal deposition are laser or electron beam power density, beam focus, powder or wire feed rate, *z*-range of build, transverse velocity of droplet deposition, *xy*-hatch spacing, and *z* increment. These parameters are not very different from those used for laser or electron beam welding, especially if it involves multi-pass welding. It is essential to have optimal control of process parameters, however, in order to achieve tighter dimensional tolerances, reasonable surface finish, and control of thermal stress. Excessive thermal stress can result in cracking and delamination between layers. In addition, it is necessary that manufacturing processes are reliable so that quality parts can be produced consistently. Accordingly, the goals of layer-by-layer manufacturing are to determine the "build envelope" and to achieve "closed loop process control" for the fabrication of high quality parts and components for critical applications. One way to achieve these goals is to develop analysis methods for determining the thermal fields, temperature histories, and fluid flow fields within close proximity of the melt pools and solidified layers. From this type of analysis, process-control algorithms can be determined for specific materials and processes.

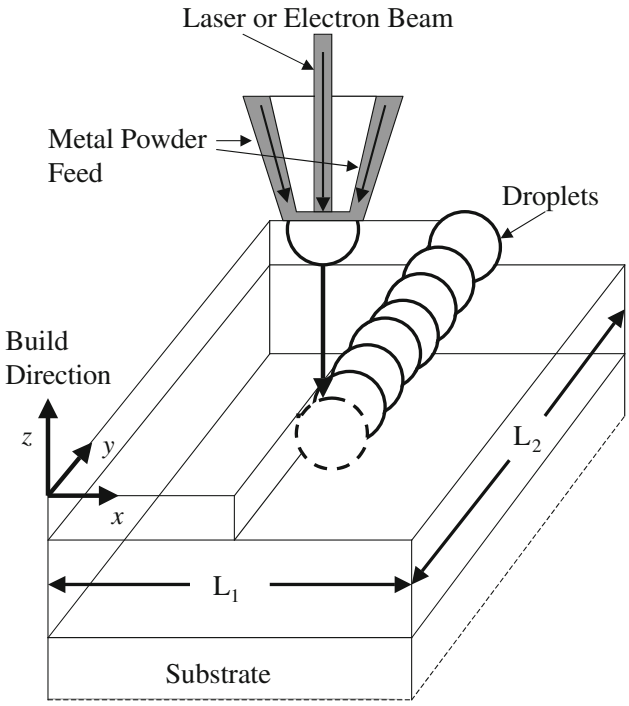

Fig. 1 Schematic representation of droplet-by-droplet deposition process showing overlapping of melt bead droplets to build a three-dimensional metallic structure

General microstructural features of metallic structures fabricated by layer-by-layer deposition processes were examined in Ref 8 and 9. Metallic structures fabricated by droplet-by-droplet liquid-metal deposition appear as a series of beads arranged side by side and one above the other. For these structures, the solidification bands are highlighted by segregation and define the shape of the melt pool. These bands also appear to correspond to the ripples on the surface. The shape of the bands suggests a flat-bottomed melt pool, which is very different from the usual hemispherical shape of melt pools occurring in welds. This suggests that most of the heat transfer in the freeformed metallic structure is through the previous layers and substrate. The band-free top region of the metallic structure consists of the last melt bead droplets to solidify. This suggests a spherical melt pool shape which is several times larger than the band spacing or layer thickness, and that considerable remelting of the previous layers takes place. The microstructure of coupon cross sections (Fig. 2) typically shows three distinct regions, a heat-affected-zone (HAZ) in the substrate, banding in the body of the deposit, and a band-free top layer.

The inherent complexity of layer-by-layer deposition processes demonstrated by various fabrication techniques establishes that modeling of heat transfer in such processes represents a relatively difficult task (Ref 1-9). This is expected to be especially the case when modeling such processes using basic theory or modeling based on first principles. That is to say, when modeling layer-by-layer deposition processes using the direct-problem approach. As discussed previously (Ref 9), a general approach to overcoming modeling difficulties associated with the inherent complexity of energy deposition

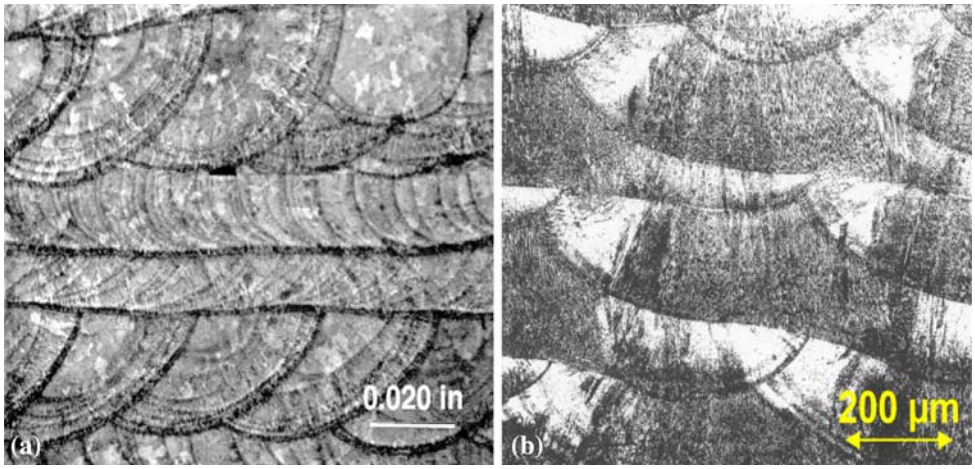

Fig. 2 Examples of microstructure showing overlapping melt bead droplets. (a) Laser-powder deposited (*Courtesy*: William Hofmeister, Vanderbilt University.) (b) E-beam-wire deposited (*Courtesy*: Thomas Eagar, MIT)

processes is the inverse problem approach. Methods of inverse analysis, in contrast to analysis methods based on the direct-problem approach, are characterized by many properties that follow directly from the fact that inverse methods are data driven as well as model driven (Ref 10, 11). Principal among these properties is the fact that relatively complex and highly nonlinear systems can be represented accurately by means of model representations characterized by small numbers of parameters. In many cases, the errors that are introduced by approximations underlying an inverse model, and its associated relatively small set of parameters, are in fact compensated for by the characteristics of the available experimental data, i.e., the data space.

In previous studies (Ref 8, 9), the concept, or more appropriately the notion, of using inverse analysis to model droplet-by-droplet liquid-metal deposition was given a preliminary examination. The numerical simulations presented in these studies demonstrated the potential feasibility of applying inverse analysis to processes involving droplet-by-droplet deposition. These studies considered, however, numerical procedures whose general methodology was not defined precisely and case study analyses of structures characterized by relatively simple geometries and boundary conditions, i.e., structures where heat conduction is essentially two dimensional in character. In this study, an algorithmic structure is presented that establishes the general applicability of inverse analysis to droplet-by-droplet liquid-metal deposition and provides for the consideration of different types of geometries and boundary conditions. This algorithmic structure, which represents an extension and refinement of an algorithmic structure presented previously (Ref 9), is readily adaptable to analysis of complex geometries where heat conduction is three dimensional in character, e.g., structures whose basic layered elements are rectangular coupons, and the formulation of process-control algorithms for process optimization.

In what follows the statement of a specific inverse problem is presented that establishes the foundation of an algorithmic structure for inverse modeling of unsteady heat conduction that occurs during droplet-by-droplet liquid-metal deposition. It is significant to note that the statement of the inverse problem presented here is more well defined than that presented previously (Ref 9) for the inverse analysis of droplet-by-droplet liquid-metal deposition. The problem statement provides a foundation for the construction of a relatively general algorithmic structure having a relatively small number of model parameters, and accordingly, the convenient and practical optimization of parameter values relative to a given data space consisting of temperature measurements or observations of phase transformations, e.g., solidification. A significant aspect of this algorithmic structure is that the concept of an equivalent or apparent distribution of energy sources (see Ref 25) is extended to include nonlocalized spatial distributions of energy sources representing the entire volumetric distribution of overlapping droplets as viewed from a specified set of sampling points. During the course of the development that follows the physical assumptions and mathematical approximations underlying the derivation of the general algorithmic structure are elucidated. A discussion is presented of specific aspects of the algorithmic structure within the context and objectives of the general inverse heat transfer problem. Subsequently, the algorithm is applied to the analysis of unsteady heat conduction within a prototype layer-by-layer liquid-metal deposition process involving fabrication of a coupon structure. The discussion of the results of this analysis considers their significance relative to sensitivity, boundary effects, and computational complexity. In particular, what physical characteristics of liquid-metal droplets are significant for inverse analysis, and accordingly, what characteristics of the calculated temperature field are appropriate for inverse modeling. Finally, it is emphasized that the overall context of this effort concerns investigation of unsteady heat transfer within metal structures that are fabricated using layer-by-layer deposition processes.

2. Statement of Inverse Heat Deposition Problem

The inverse problem concerning analysis of physical processes, in general (Ref 12-19), and the inverse heat transfer problem, in particular (Ref 20-24), may be stated formally in terms of source functions (or input quantities) and multidimensional fields (output quantities). The statement of the inverse problem given here, as in previous studies (Ref 9, 25), is focused on aspects of the inverse heat deposition problem that are related to the determination of temperature fields by means of appropriate regularization of their space and time distributions. This statement represents an extension of those given in Ref 24-26 and is for the specific application of inverse analysis to heat deposition processes involving droplet-by-droplet liquid-metal deposition. This statement of the inverse problem is such that the concept of an equivalent or apparent distribution of energy sources (see Ref 25) is extended to include nonlocalized spatial distributions of energy sources representing the entire volumetric distribution of overlapping droplets as viewed from a specified sampling point.

In general, the formulation of a heat conductive system occupying an open bounded domain Ω with an outer boundary S_o and an inner boundary S_i involves the parabolic equation

$$\frac{\partial T(\hat{x},t)}{\partial t} = \nabla \cdot (\kappa(\hat{x},t)\nabla T(\hat{x},t)) \qquad \text{(Eq 1a)}$$

for $T(\hat{x},t)$ in $\Omega \times (0,t_f)$, with initial condition $T(\hat{x},0) = T_0(\hat{x})$ in Ω, and heat flux exchanges through the outer and inner boundaries S_o and S_i as follows:

$$-\kappa(\hat{x},t)\frac{\partial T(\hat{x},t)}{\partial n_{S_o}} = c(\hat{x},t)(T(\hat{x},t) - T_a(\hat{x},t)) \qquad \text{(Eq 1b)}$$

on $S_o \times (0,\ t_f)$, and

$$-\kappa(\hat{x},t)\frac{\partial T(\hat{x},t)}{\partial n_{S_i}} = q(\hat{x},t) \qquad \text{(Eq 1c)}$$

on $S_o \times (0,\ t_f)$. Here $\hat{x} = (x,y,z)$ is the position vector, n_{S_o} and n_{S_i} are the normal vectors onto boundaries S_o and S_i, respectively, t is the time variable, t_f is the final time, $T(\hat{x},t)$ is the temperature field variable, $\kappa(\hat{x},t)$ is the thermal diffusivity field variable, $c(\hat{x},t)$ and $T_a(\hat{x},t)$ are specified functions, and $q(\hat{x},t)$ is the heat flux on the inner boundary S_i. Determination of the temperature field by solution of Eq 1(a-c) defines the direct initial-boundary value problem. The statement of the inverse problem considered here, whose generalization is also considered, is that of effectively reconstructing the heat flux field $q(\hat{x},t)$ on the inner and outer boundaries S_i and S_o, and the resulting temperature field $T(\hat{x},t)$ for all time $t \in [0,t_f]$, when

S_i and S_o are totally or partially inaccessible. In order to reconstruct the heat flux, information concerning the temperatures $T(\hat{x}_s, t)$, where $\{\hat{x}_s\} \in S_i, S_o$ is needed and therefore must be acquired either experimentally or via direct numerical simulation (Ref 26).

Following the inverse analysis approach, a parametric representation based on a physical model provides a means for the inclusion of information concerning the physical characteristics of a given energy deposition process. It follows then that for heat deposition processes involving the deposition of heat within a bounded region of finite volume, a consistent parametric representation of the temperature field is given by

$$T(\hat{x}, \kappa, t) = T_A + \sum_{k=1}^{N_k} T_k(\hat{x}, \hat{x}_k, \kappa, t; \alpha_1, \ldots, \alpha_n) \quad \text{(Eq 2a)}$$

and

$$T(\hat{x}_n^c, t_n^c, \kappa) = T_n^c \quad \text{(Eq 2b)}$$

where the quantity T_A is the ambient temperature of the workpiece and the locations $\hat{x}_n^c$ and temperature values T_n^c specify constraint conditions on the temperature field. The functions $T_k(\hat{x}, \hat{x}_k, \kappa, t; \alpha_1, \ldots, \alpha_n)$ represent an optimal basis set of functions for given sets of boundary conditions and material properties. The quantities $\hat{x}_k = (x_k, y_k, z_k)$, $k = 1,\ldots, N_k$, are the locations of the elemental source or boundary elements. The sum defined by Eq 2a can for certain systems specify numerical integration over the discrete elements of a distribution of sources or boundary elements. Selection of an optimal set of basis functions is based on a consideration of the characteristic model and data spaces of heat deposition processes and subsequently isolating those regions of the model space corresponding to parameterizations that are both physically consistent and sufficiently general in terms of their mathematical representation and mapping from data to model space (see Ref 25, 26). Although heat deposition processes may be characterized by complex coupling between the heat source and workpiece, as well as complex geometries associated with either the workpiece or deposition process, in terms of inverse analysis the general functional forms of the temperature fields associated with all such processes are within a restricted class of functions, i.e., optimal sets of functions. Accordingly, a sufficiently optimal set of functions are the analytic solutions to heat conduction equation for a finite set of boundary conditions (Ref 27). A parameterization based on this set is both sufficiently general and convenient relative to optimization.

The formal procedure underlying the inverse method considered here entails the adjustment of the temperature field defined over the entire spatial region of the sample volume at a given time t. This approach defines an optimization procedure where the temperature field spanning the spatial region of the sample volume is adopted as the quantity to be optimized. The constraint conditions are imposed on the temperature field spanning the bounded spatial domain of the workpiece by minimization of the value of the objective functions defined by

$$Z_T = \sum_{n=1}^{N} w_n \left(T(\hat{x}_n^c, t_n^c, \kappa) - T_n^c\right)^2 \quad \text{(Eq 3)}$$

where T_n^c is the target temperature for position $\hat{x}_n^c = (x_n^c, y_n^c, z_n^c)$.

The input of information into the inverse model defined by Eq 1-3, i.e., the mapping from data to model space, is effected by: the assignment of individual constraint values to the quantities T_n^c; the form of the basis functions adopted for parametric representation; and specifying the shapes of the inner and outer boundaries, S_i and S_o, respectively, which bound the temperature field within a specified region of the workpiece. The constraint conditions and basis functions, i.e., $T(\hat{x}_n^c, t_n^c, \kappa) = T_n^c$ and $T_k(\hat{x}, \hat{x}_k, \kappa, t; \alpha_1, \ldots, \alpha_n)$, respectively, provide for the inclusion of the following types of information: (a) solidification cross sections; (b) spatial character of energy source (e.g., position of maximum temperature, shape, and relative location of melt pool); (c) geometric information (e.g., shape features of the metallic structure); (d) boundary conditions on the structure; (e) information related to temperature history (e.g., microstructure correlation with temperature); (f) thermocouple measurements; (g) energy input (e.g., energy per distance); and (h) information based on physical model representations of aspects of heat deposition process.

A general parametric representation of heat deposition processes follows from a set of general properties. First, the general trend features of heat deposition processes are such that the construction of a complete basis set of functions $T_k(\hat{x}, \hat{x}_k, \kappa, t; \alpha_1, \ldots, \alpha_n)$ making up a linear combination of the form defined by Eq 2 for representation of the associated temperature field is well defined and readily achievable. Second, for heat deposition processes, characteristics of the temperature field are poorly correlated to characteristics of the energy source. The characteristics of the temperature field that are associated with these processes, however, are strongly coupled only to inner boundary S_i on this field, e.g., the solidification boundary. This property follows from the low-pass spatial filtering property of the basis functions $T_k(\hat{x}, \hat{x}_k, \kappa, t; \alpha_1, \ldots, \alpha_n)$, whose general forms are consistent with the dominant trend features of heat deposition processes (Ref 25). Third, given a consistent set of basis functions, the temperature field associated with a heat deposition process is completely specified by: the shape and temperature distribution

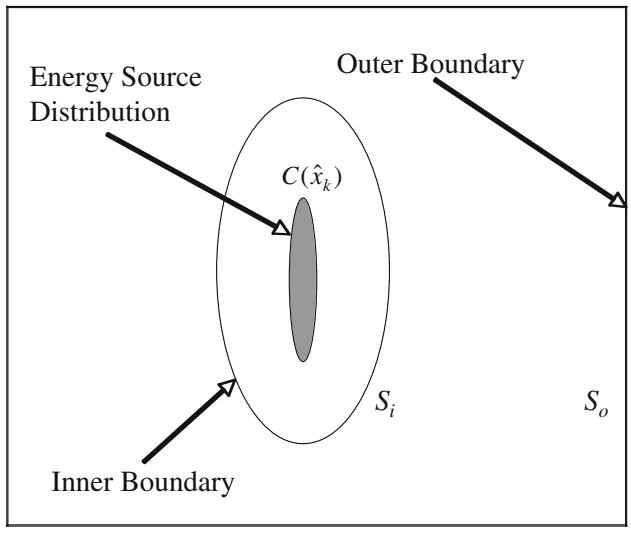

Fig. 3 Two-dimensional schematic representation of inner and outer boundaries of temperature field that define inverse heat transfer problem

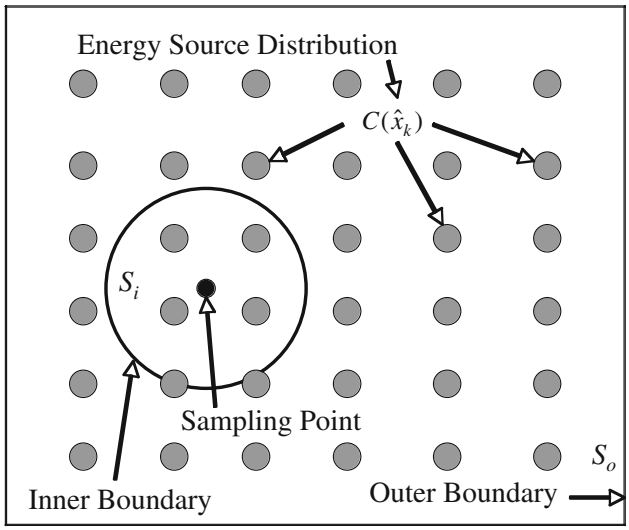

Fig. 4 Two-dimensional schematic representation of inner and outer boundaries of temperature field that define inverse heat transfer problem with respect to a sampling point in a closed region bounded by surface S_i that is contained within a volumetric distribution of heat sources bounded by S_o

of a given inner boundary S_i on the domain of the temperature field; the diffusivity κ; and the lengths of the spatial dimensions of the structure. Fourth, the shape and temperature distribution of a specified inner boundary S_i is determined by the rate of energy deposited within the volume of the structure. And finally, in that an inner boundary S_i (see Fig. 3) is defined by its shape and the distribution of temperatures on its surface $T(\hat{x}_S)$, it follows that one can define a multidimensional temperature field $T(\hat{x}, \kappa, V, D_i, T(\hat{x}_S), \hat{x}_S \in S_i)$. In doing so, referring to Fig. 3, the inverse problem defined by the mapping

$$C(\hat{x}_k) \mapsto T(\hat{x}) \qquad \text{(Eq 4)}$$

can be replaced by the inverse problem defined by the mapping

$$C(\hat{x}_k), \kappa \mapsto S_i, S_0 \mapsto T(\hat{x}) \qquad \text{(Eq 5)}$$

Following the same arguments, the definition of the inverse heat deposition problem as given above can be extended to include systems that are characterized by incomplete information concerning the diffusivity function κ. This would include any nonlinear dependence of κ on temperature. This follows in that Eq 5 implies the existence of a weighted space averaged diffusivity.

At this stage, the statement of the inverse heat deposition problem given above can be generalized to provide for the construction of a parametric representation of droplet-by-droplet liquid-metal deposition. This generalization is represented schematically in Fig. 4 where the region of interest for determination of the temperature field is contained within a volumetric distribution of heat sources bounded by S_o. Referring to Fig. 4, the generalization of the inverse problem represented by Fig. 3 is that of effectively reconstructing the heat flux field $q(\hat{x}, t)$ on the inner and outer boundaries S_i and S_o, and the resulting temperature field $T(\hat{x}, t)$ for all time $t \in [0, t_f]$ at points $\hat{x}_p$ within the inner boundary S_i, when the heat source distribution $C(\hat{x}_k)$ is specified, in addition to total or partial information concerning S_i and S_o.

3. Formulation of General Algorithm

In that the droplet-by-droplet liquid-metal deposition process can, in general, be characterized by two separate spatial domains corresponding to the distribution of discrete droplet sources and the temperature field distribution within the neighborhood of each sampling point, it follows that a consistent representation of the temperature field in terms of basis functions is of the form

$$T(\hat{x}, t) = T_A + \sum_{k=1}^{N_k} \sum_{n=1}^{N_t} C(\hat{x}_k, n\Delta t) F_k^{(d)}(\hat{x}, \hat{x}_k, n\Delta t, \kappa) \qquad \text{(Eq 6)}$$

where $t = N_t \Delta t$ and the functions $F_k^{(d)}(\hat{x}, \hat{x}_k, t, \kappa)$ are given by

$$F_k^{(3)}(\hat{x}, \hat{x}_k, t, \kappa) = \frac{1}{(t)^{3/2}} \exp\left[-\frac{(x-x_k)^2 + (y-y_k)^2 + (z-z_k)^2}{4\kappa t}\right] \qquad \text{(Eq 7)}$$

for heat diffusion whose general trend is characteristically three dimensional,

$$F_k^{(2)}(\hat{x}, \hat{x}_k, t, \kappa) = \frac{1}{t} \exp\left[-\frac{(x-x_k)^2 + (y-y_k)^2}{4\kappa t}\right] \times \left\{1 + 2\sum_{m=1}^{\infty} \exp\left[-\frac{\kappa m^2 \pi^2 t}{l^2}\right] \cos\left[\frac{m\pi z}{l}\right] \cos\left[\frac{m\pi z_k}{l}\right]\right\} \qquad \text{(Eq 8)}$$

for heat diffusion whose general trend is characteristically two dimensional, and

$$F_k^{(1)}(\hat{x}, \hat{x}_k, t, \kappa) = \frac{1}{\sqrt{t}} \exp\left[-\frac{(x-x_k)^2}{4\kappa t}\right] \times \left\{1 + 2\sum_{m=1}^{\infty} \exp\left[-\frac{\kappa m^2 \pi^2 t}{a^2}\right] \cos\left[\frac{m\pi y}{a}\right] \cos\left[\frac{m\pi y_k}{a}\right]\right\} \times \left\{1 + 2\sum_{m=1}^{\infty} \exp\left[-\frac{\kappa m^2 \pi^2 t}{l^2}\right] \cos\left[\frac{m\pi z}{l}\right] \cos\left[\frac{m\pi z_k}{l}\right]\right\} \qquad \text{(Eq 9)}$$

for heat diffusion whose general trend is characteristically one dimensional. The "dimensionality" of the functions $F_k^{(d)}(\hat{x}, \hat{x}_k, t, \kappa)$ is selected according to the relative proximity of a given set of sampling points to one or more nonconducting boundaries. The influence of nonconducting boundaries based on the relative proximity of sampling points is represented schematically in Fig. 5. Referring to this figure, it follows that calculation of the temperature field at sampling points within regions A, B, and C would adopt the basis functions $F_k^{(d)}(\hat{x}, \hat{x}_k, t, \kappa)$ defined by Eq 9, 7, and 8, respectively.

At this point, some of the basic mathematical elements underlying the general algorithmic structure presented above for inverse modeling of droplet-by-droplet liquid-metal deposition are reviewed. This algorithmic structure is based on the parametric representation of the time-dependent temperature field that is defined by Eq 6 to 9. For droplet-by-droplet liquid-metal deposition, spatial filtering properties are perceived intuitively by the observation that the diffusion of heat within a structure that is being built is insensitive to many of the details associated with specific shape features of a given melt bead droplet and, for many locations within the structure,

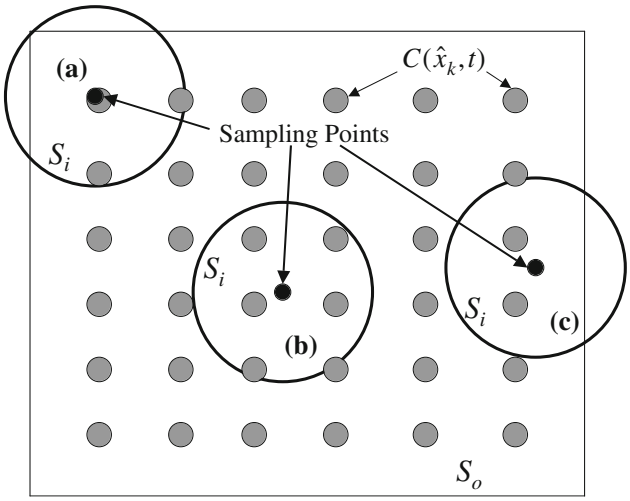

Fig. 5 Two-dimensional schematic representation of sampling points having different types of local influences. (a) Temperature field is sensitive to source distribution and as well as the influence of two (or three) nonconducting boundaries. (b) Temperature field is sensitive to source distribution only. (c) Temperature field is sensitive to source distribution and as well as the influence of a single nonconducting boundary

influences of physical boundaries. These filter properties were examined rigorously in Ref 9 and follow from the fact that the spatial Fourier transform of the dominant trend factor of the basis functions $F_k^{(d)}(\hat{x}, \hat{x}_k, t, \kappa)$ defined by Eq 7 to 9,

$$f_t(x) = \exp\left[-\frac{(x - x_k)^2}{4\kappa t}\right], \qquad \text{(Eq 10)}$$

is within the class of low-pass spatial filter functions whose range of filtered spatial modes increases with time t. This filtering is with respect to spatial modes associated with both the spatial distribution of the coefficients $C(\hat{x}_k, n\Delta t)$, and factors making up the functions $F_k^{(d)}(\hat{x}, \hat{x}_k, t, \kappa)$ that represent the influence of nonconducting boundaries. These filter properties establish conditions that provide for relative reduction in the number of parameters that are required for representation of spatial features associated with both melt bead droplets and boundaries. In addition, these filter properties provide for a reduction of algorithm complexity (see Ref 9). This follows in that spatial filtering provides conditions such that the calculation of temperature histories at a finite number of sample points, in contrast to the entire volume of the structure, results in a significant reduction of computational cost. The general algorithmic formulation defined by Eq 6-9, which is possible because of spatial filtering, is such that the concept of an equivalent or apparent distribution of energy sources is extended to include nonlocalized spatial distributions of energy sources representing the entire discrete volumetric distribution of overlapping droplets as viewed from a specified sampling point (see Fig. 4).

4. Prototype Analysis

In this section, a prototype analysis is presented that demonstrates application of the general algorithmic structure presented above to the inverse analysis of layer-by-layer deposition processes and provides for an examination of mathematical properties underlying the algorithmic formulation. The prototype system is that of the freeform fabrication of a rectangular coupon for a system whose thermal diffusivity is within the range of steel. The model system consists of a sequence layer, where each layer consists of a surface distribution of discrete energy sources whose strengths are assigned by the values of the coefficients $C(\hat{x}_k, n\Delta t)$ defined in Eq 6 and are numerically integrated, or summed discretely, at each time step. Each of the discrete energy sources represents a discrete liquid-metal droplet of a given volume. The translation speed of the sample relative to the point of liquid-metal deposition is assigned implicitly through the time dependence and relative locations of the discrete energy sources, $C(\hat{x}_k, n\Delta t)$. That is to say, a certain number of drops per layer and a certain number of layers as a function of time are specified. The model parameters used for the prototype analysis are listed in Table 1. For purposes of this analysis, the basis function $F_k^{(d)}(\hat{x}, \hat{x}_k, t, \kappa)$ given by Eq 8 is adopted for calculation of the temperature field. These functions are the solution to the heat conduction equation for a temperature independent diffusivity and nonconducting boundaries on two surfaces that are separated by a distance l, which will correspond to the thickness of the coupon to be fabricated. Accordingly, it is assumed for this simulation that there is no conduction at the substrate boundary. An additional condition imposed on the model system is that of heat transfer into the ambient environment at the edges of the rectangular coupon being fabricated. This is a realistic assumption for process conditions where droplet-by-droplet deposition occurs within a mold structure consisting of a metal powder composite whose thermal diffusivity is similar to that of the fabricated structure, e.g., rectangular coupon. A constraint condition imposed on the temperature field is that the liquid-solid interface defined by the alloy liquidus temperature is at 1430 °C, consistent with thermal properties of steel. Accordingly, the values assigned to the coefficients $C(\hat{x}_k, n\Delta t)$ were such that the average temperature of each discrete droplet was within the range of liquid metal. It is significant to note that other constraint conditions such as melt pool dimensions and measurements of temperature via thermocouples can also be adopted for assigning values to the coefficients $C(\hat{x}_k, n\Delta t)$. In the present prototype analysis, the layers are deposited one on top of the other by traversing the passes in a zig-zag fashion according to different types of layer-by-layer and droplet-by-droplet deposition sequences. Consistent with the filter properties associated with thermal diffusion, each melt bead droplet can be represented by a cube

Table 1 Model Parameters Used to Determine Thermal Fields in Layer-by-Layer Deposition Process

Model parameters
Material: steel
Diffusivity: $\kappa = 2.5 \times 10^{-5}$ m^2/s
Time step: $\Delta t = 0.001$ s
Drop deposited every 20 time steps
49 drops per layer
Droplet energy content: $C(\hat{x}_k, n\Delta t) = 4.0$
Droplet volume = $(\Delta l)^3$, $\Delta l = 0.2$ cm

(see Table 1). This follows in that the filtering of fine spatial structure due to the dominant trend factor Eq 10 implies that the temperature field is insensitive to details of the shape of the melt bead droplet. It is significant to note, however, that the temperature field is sensitive to the spatial distribution of droplets (see Ref 9). The prototype analysis considers calculation of the temperature field at sampling points within two different regions of the model structure. Shown in Fig. 6 is schematic representation of relative locations of these sampling points with respect to the substrate surface, the spatial domain defining a rectangular coupon, and the build direction. Shown in Fig. 7 are different types of droplet-by-droplet deposition sequences. These different droplet-by-droplet deposition sequences, used in different combinations, define different types of layer-by-layer deposition sequences. Before proceeding, it is to be noted that the model parameters given in Table 1 are such that the time for deposit of each layer is 0.98 s.

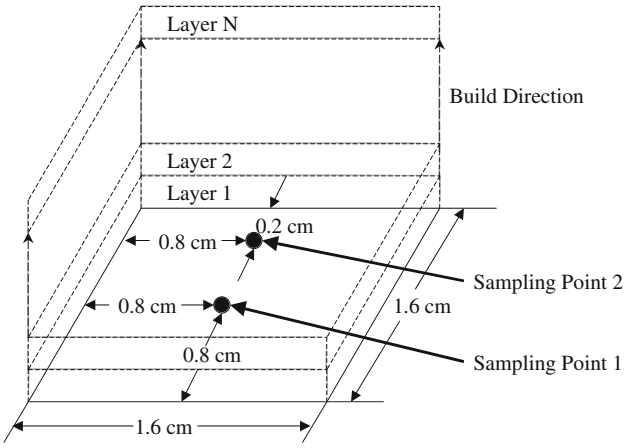

Fig. 6 Schematic representation of relative locations of sampling points with respect to surface of substrate, spatial domain defining rectangular coupon, and build direction

Shown in Fig. 8-10 are the time evolution of the temperature field for the layer-by-layer deposition sequences (AAA…), (ABAB…), and (ACAC…), respectively, defined according to the different droplet-by-droplet deposition sequences defined in Fig. 7. Each of the subfigures in Fig. 8-10 consist of a two-dimensional slice of the calculated three-dimensional temperature field at the nonconducting substrate boundary at different time. It should be noted that calculation of the temperature field over two-dimensional slices is for the purpose of examining properties of the algorithm. In practice, for extended periods of time, the temperature field determined

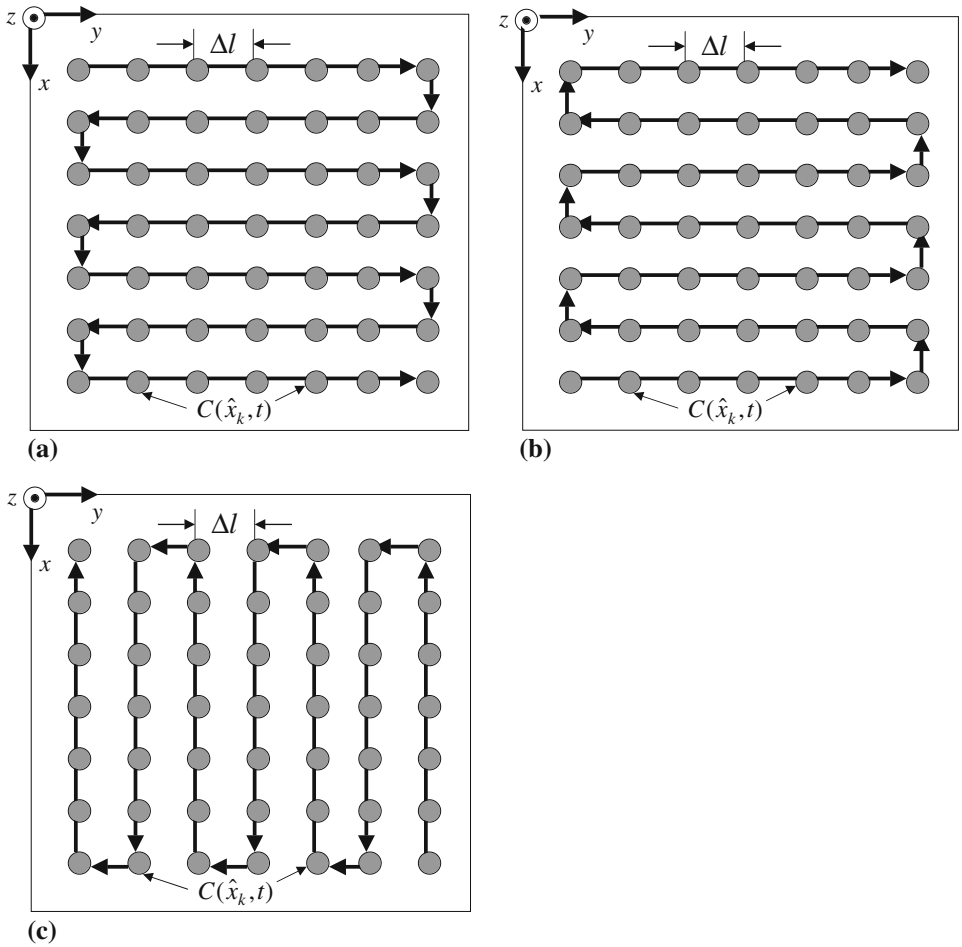

Fig. 7 Three different droplet-by-droplet deposition sequences per layer used in numerical simulations, where droplet volume is $(\Delta l)^3$ and Δl = 0.2 cm. The layer-by-layer deposition sequence (ACAC…) represents a continuous path

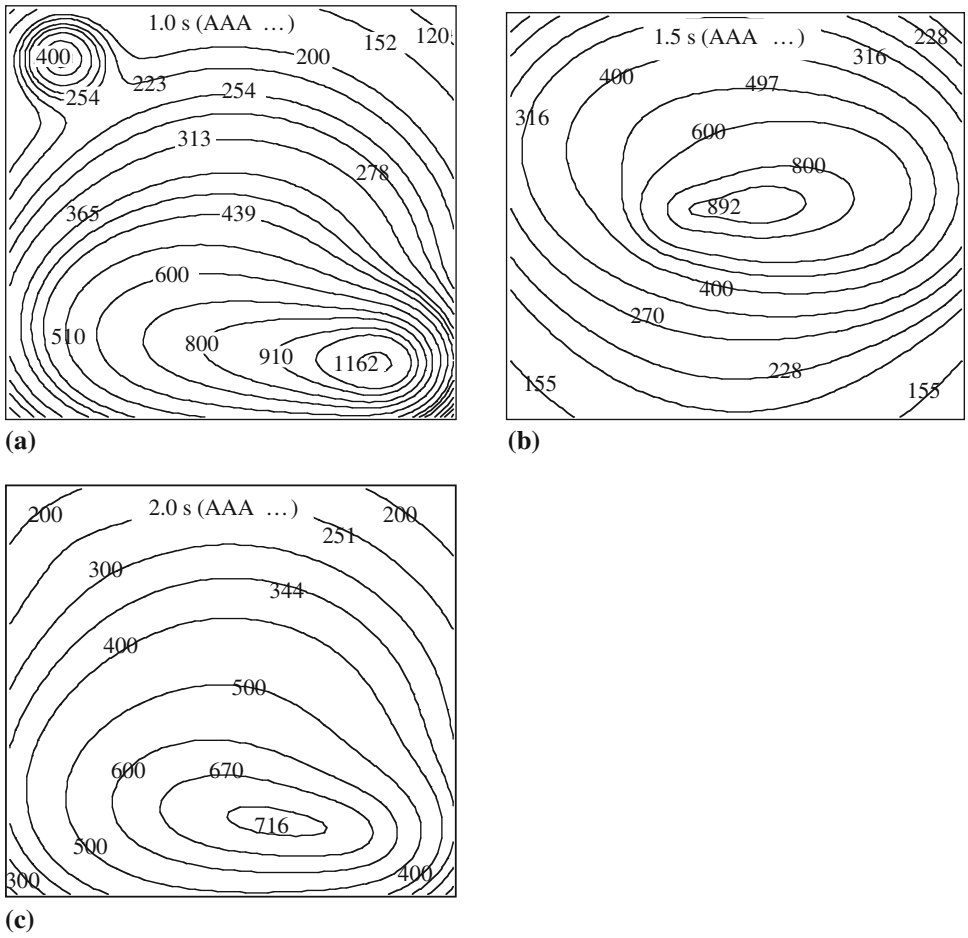

Fig. 8 Temperature field in units of °C as a function of time at nonconducting substrate boundary for layer-by-layer deposition sequence (AAA…) defined according to Fig. 7

more conveniently at a finite number of sample points thus significantly reducing the complexity of the algorithm such that its computational cost scales only as the number of droplets. Referring to Fig. 8-10, one notes the temperature distribution within the neighborhood of an individual droplet for a time period corresponding to the duration of its deposit. This temperature distribution, and the associated local time evolution of the solid-liquid interface, represents one of the primary constraints on the calculated temperature field. The local temperature distribution of an individual droplet provides for the implicit specification of the rate of energy deposition into the system. Accordingly, the entire temperature history can be scaled according the evolution of the solid-liquid boundary that is observed for an individual droplet that is deposited upon a metal surface. For example, referring to Fig. 8(a), 9(b), and 10(a), one can observe in each figure the location of the last droplet deposited. In each of these simulations, the size of the melt pool associated with each droplet can be specified by adjusting the scale of the entire temperature field relative to the alloy liquidus temperature, e.g., 1430 °C. In addition, referring to Fig. 8-10 at times greater than 1.0 s, the local time evolution of the solid-liquid interface can be adjusted according to experimentally observed remelting of previously deposited layers.

Shown in Fig. 11 are the temperature histories calculated at sample point 1 indicated in Fig. 6 for layer-by-layer sequences (AAA…), (ABAB…), and (ACAC…) defined according to Fig. 7. As seen in this figure, the temperature histories at this point are identical in that the amount of heat transferred to this point as a function of time is the same for all three layer-by-layer sequences.

Shown in Fig. 12-14 are the temperature histories calculated at sample point 2 indicated in Fig. 6 for layer-by-layer sequences (AAA…), (ABAB…), and (ACAC…), respectively, defined according to Fig. 7. Comparison of these temperature histories provides an example of establishing correlation between microstructure, which is correlated with phase transformations, and process control. For this prototype analysis, the relative level of reheating of the first layer is considered. Accordingly, it can be observed that the sequences (AAA…) and (ACAC…) result in a reheating of the first layer (at sampling point 2) that is on average higher than that of the sequence (ABAB…). The sequence (ABAB…), however, results in a reheating of the first layer that assumes a larger maximum temperature than that of the other sequences.

Another aspect of process control that is of significance for droplet-by-droplet deposition is the relative degree of

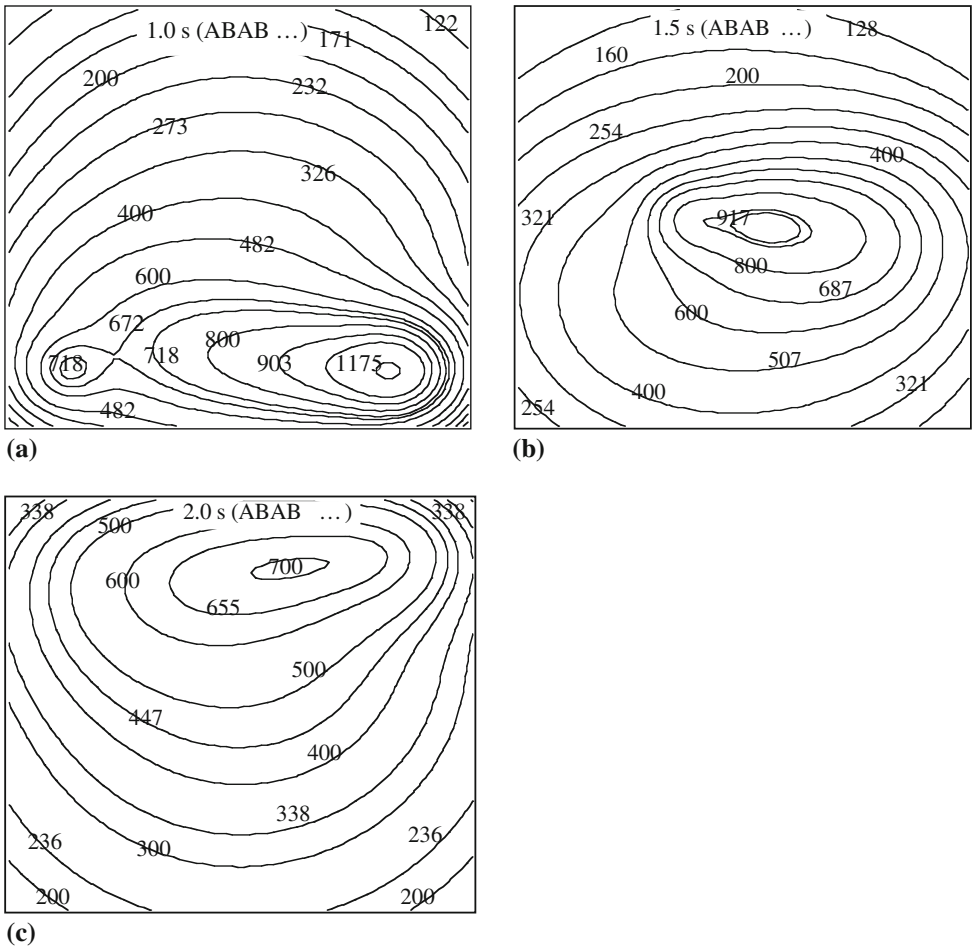

Fig. 9 Temperature field in units of °C as a function of time at nonconducting substrate boundary for layer-by-layer deposition sequence (ABAB…) defined according to Fig. 7

continuity of the path for liquid-metal deposition. The relative degree of deposition-path continuity will influence both the temperature histories at various regions within the fabricated structure as well as the control algorithm adopted by an automated process planner for imposing the trajectory of each droplet. For example, the layer-by-layer sequences (AAA…), (ABAB…), and (ACAC…) defined according to Fig. 7 are characterized by different levels of deposition-path continuity. Accordingly, the deposition sequence (AAA…) represents the most discontinuous path, while the deposition sequence (ACAC…) defines a completely continuous path.

5. Conclusion

The success of fabrication processes based on layer-by-layer liquid-metal deposition will depend upon the degree of reliability of the manufacturing technology. For this, it is important to have reliable predictability of temperature histories and then to relate these histories to parameters associated with process control. The general algorithmic structure presented here, which addresses this goal, represents an extension and refinement of an algorithmic structure presented previously for inverse modeling of layer-by-layer liquid-metal deposition. This algorithmic structure is potentially adaptable for prediction of temperature histories within fabricated parts having complex geometries and for the construction of process-control algorithms. The specific aspect of the algorithmic structure, in terms of numerical analysis, which provides for its adaptability to complex geometries is that the model system entails a contiguous discrete distribution of active heat sources. The prototype analysis presented here demonstrates application of the general algorithmic structure. This prototype analysis, however, considered a specific set of system boundary conditions. Accordingly, further analysis is required to address issues related to the sensitivity and general dependence of temperature histories on changes in boundary conditions and process parameters. Changes in process parameters could include changes in the path of sequential droplet deposition and variations in droplet size during deposition. Finally, optimal process control will require correlation of temperature histories with microstructure. Further study and algorithm extension are required to address this issue.

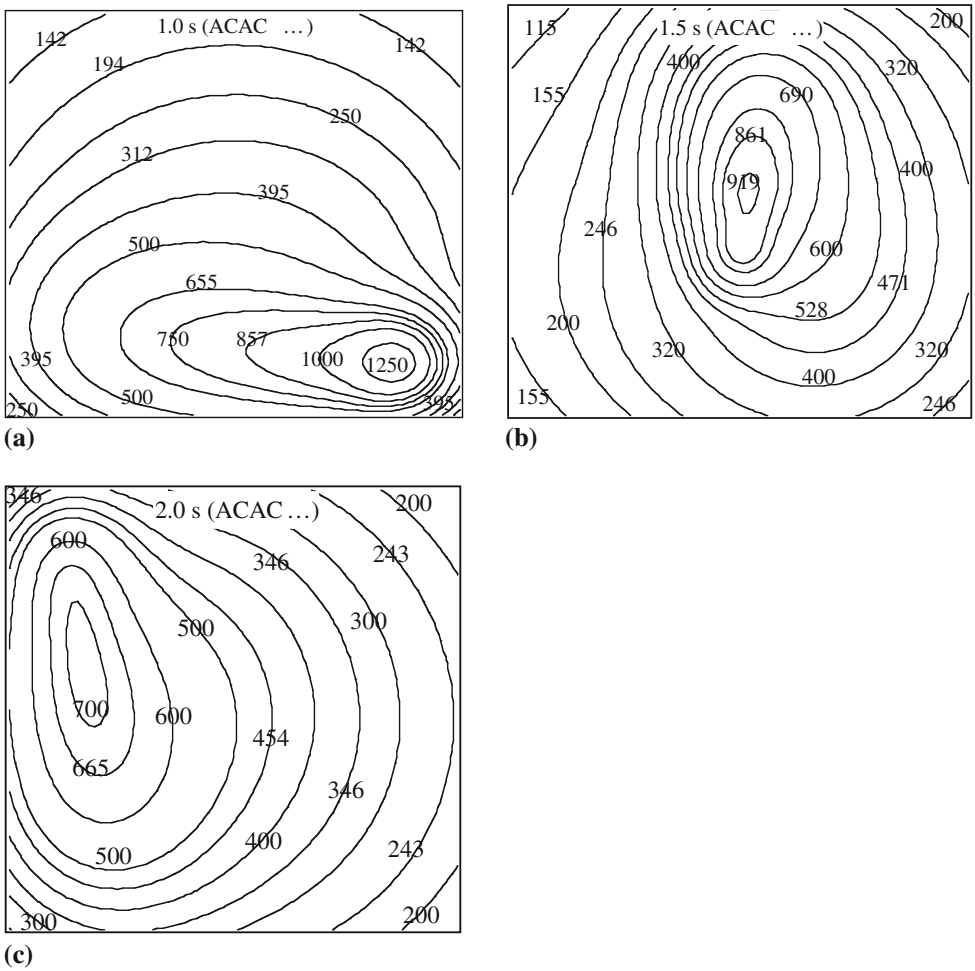

Fig. 10 Temperature field in units of °C as a function of time at nonconducting substrate boundary for layer-by-layer deposition sequence (ACAC…) defined according to Fig. 7

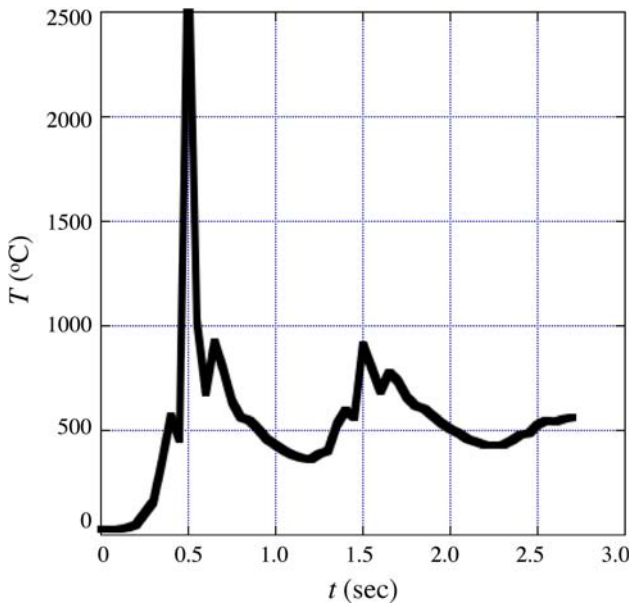

Fig. 11 Temperature histories calculated at sample point 1 indicated in Fig. 6 for layer-by-layer sequences (AAA…), (ABAB…), and (ACAC…) defined according to Fig. 7

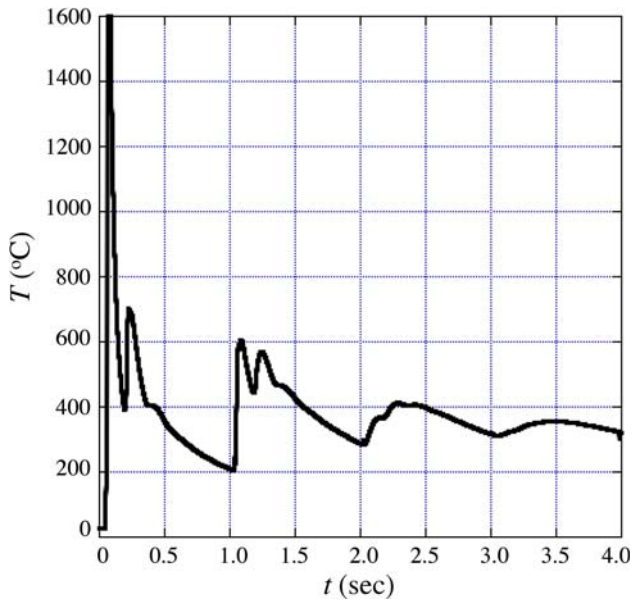

Fig. 12 Temperature history calculated at sample point 2 indicated in Fig. 6 for layer-by-layer deposition sequence (AAA…) defined according to Fig. 7

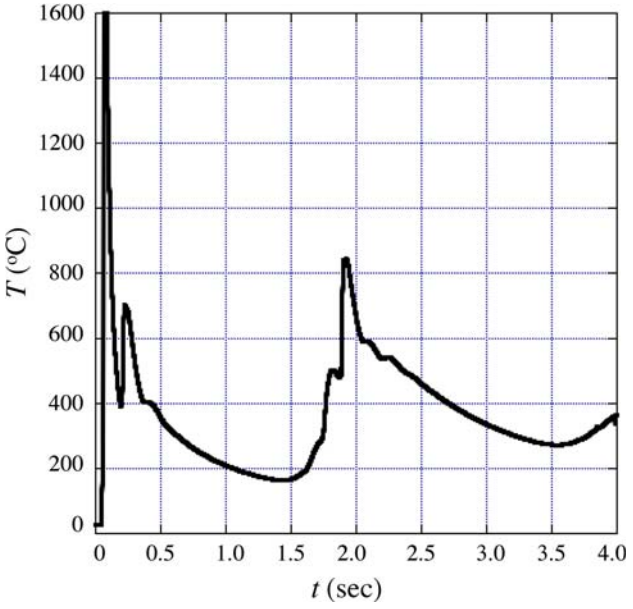

Fig. 13 Temperature history calculated at sample point 2 indicated in Fig. 6 for layer-by-layer deposition sequence (ABAB…) defined according to Fig. 7

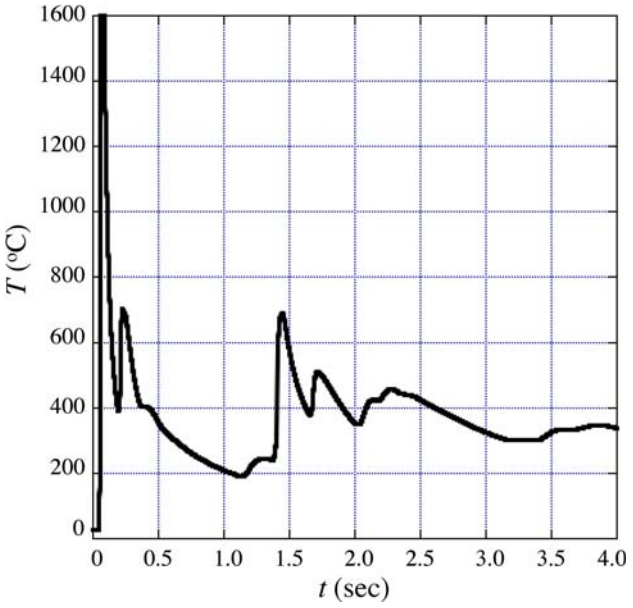

Fig. 14 Temperature history calculated at sample point 2 indicated in Fig. 6 for layer-by-layer deposition sequence (ACAC…) defined according to Fig. 7

Acknowledgment

This work was supported by the Office of Naval Research.

References

1. K.P. Cooper, Layered Manufacturing: Challenges and Opportunities, *Mat. Res. Soc. Symp. Proc.*, 2003, **758**, p LL1.4.1
2. M.L. Griffith, D.M. Keicher, and C. L. Atwood, Fabrication of Metallic Components using Laser Engineered Net Shaping (LENS), *Proceedings of SFF Symposium*, University of Texas-Austin, Austin, TX, 1996, p 125
3. P. Chavez, From the Inside Out: The LENS™ Process is Fueling a Paradigm Shift in Modern Manufacturing Applications, *Technical Brief*, Optomec, Inc., 2000
4. F.G. Arcella and F.H. Froes, Producing Titanium Aerospace Components from Powder Using Laser Forming, *JOM*, 2000, **52**(5), p 28
5. K.M.B. Taminger, R.A. Hafley, and D.L. Dicus, Solid Freeform Fabrication: An Enabling Technology for Future Space Missions, *Proceedings of the 2002 International Conference on Metal Powder Deposition for Rapid Manufacturing*, MPIF, Princeton, NJ, 2002, p 51
6. W. Hofmeister, M. Wert, J. Smugeresky, J.A. Philliber, M. Griffith, and M. Ensz, Investigating Solidification with the Laser-Engineered Net Shaping (LENS™) Process, *JOM-e*, 1999, **51**(7)
7. J. Beuth and N. Klingbeil, The Role of Process Variables in Laser-Based Direct Metal Solid Freeform Fabrication, *JOM*, 2001, **53**(9), p 36
8. K.P. Cooper and S.G. Lambrakos, Fabrication of Net-Shaped Metallic Parts by Overlapping Reinforcement Weld Beads, *Proceedings of the Seventh International Conference on Trends in Welding Research*, ASM International, Materials Park, OH, 16-20 May, Pine Mountain, GA, 2005, p 647
9. S.G. Lambrakos and K.P. Cooper, An Algorithm for Inverse Modeling of Layer-by-Layer Deposition Processes, *JMEP*, 2009, **18**, p 221-230
10. J. Michopoulos and S. Lambrakos, On the Fundamental Tautology of Validating Data-Driven Models and Simulations, *Int. Conf. Comput. Sci.*, 2005, **2**, p 738–745
11. J.G. Michopoulos and S.G. Lambrakos, Underling Issues Associated with Validation and Verification of Dynamic Data Driven Simulation, *Proceedings of the 2006 Winter Simulation Conference*, 3-6 Dec 2006 (Monterey, CA), L.F. Perrone, F.P. Wieland, J. Liu, B.G. Lawson, D.M. Nicol, and R.M. Fujimoto, Ed., 2006, CD-ROM, ISBN 1-4244-0501-7, IEEE Catalog Nu. 06CH37826
12. D.N. Ghosh Roy, *Methods of Inverse Problems in Physics*, Boca Raton, CRC Press, 1991
13. K.A. Woodbury, Ed., *Inverse Engineering Handbook*, CRC Press, New York, 2003
14. A. Tarantola, *Inverse Problem Theory and Methods for Model Parameter Estimation*, SIAM, Philadelphia, PA, 2005
15. C.R. Vogel, *Computational Methods for Inverse Problems*, SIAM, Philadelphia, PA, 2002
16. P.C. Sabatier, *Inverse Problems: An Interdisciplinary Study*, Academic Press, London, 1987
17. C.W. Groetsch, *Inverse Problems in the Mathematical Sciences*, Vieweg, Bruanschweig, Wiesbaden, 1993
18. A. Kirsch, *An Introduction to the Mathematical Theory of Inverse Problems*, Springer-Verlag, New York, 1996
19. A.G. Ramm, *Inverse Problems, Mathematical and Analytical Techniques with Applications to Engineering*, Springer Science, New York, 2005, p 9–10
20. M.N. Ozisik and H.R.B. Orlande, *Inverse Heat Transfer, Fundamentals and Applications*, Taylor and Francis, New York, 2000
21. K. Kurpisz and A.J. Nowak, *Inverse Thermal Problems*, Computational Mechanics Publications, Boston, USA, 1995
22. O.M. Alifanov, *Inverse Heat Transfer Problems*, Springer, Berlin, 1994
23. J.V. Beck, B. Blackwell, and C.R. St. Clair, *Inverse Heat Conduction: Ill-Posed Problems*, Wiley Interscience, New York, 1985
24. J. Xie and J. Zou, Numerical Reconstruction of Heat Fluxes, *SIAM J. Numer. Anal.*, 2005, **43**(4), p 1504–1535
25. S.G. Lambrakos and S.G. Michopoulos, Algorithms for Inverse Analysis of Heat Deposition Processes, *Mathematical Modelling of Weld Phenomena*, Vol. 8, Verlag der Technischen Universite Graz, Austria, 2007, p 847
26. S.G. Lambrakos, General Basis Functions for Parametric Representation of Energy Deposition Processes, *JMEP*, doi:10.1007/s11665-009-9368-z
27. H.S. Carslaw and J. C. Jaegar, *Conduction of Heat in Solids*, 2nd ed., Clarendon Press, Oxford, 1959, p 374